

Grass-roots optimization of coupled oscillator networks

Pranick R. Chamlagai,¹ Dane Taylor,² and Per Sebastian Skardal^{1,*}

¹*Department of Mathematics, Trinity College, Hartford, CT 06106, USA*

²*Department of Mathematics, University at Buffalo, State University of New York, Buffalo, NY 14260, USA*

Synchronization is critical for system function in applications ranging from cardiac pacemakers to power grids. Existing optimization techniques rely largely on global information, and while they induce certain local properties, those alone do not yield optimal systems. Therefore, while useful for designing man-made systems, existing theory provides limited insight into self-optimization of naturally-occurring systems that rely on local information and offer limited potential for decentralized optimization. Here we present a method for “grass-roots” optimization of synchronization, which is a multiscale mechanism involving local optimizations of smaller subsystems that are coordinated to collectively optimize an entire system, and the dynamics of such systems are particularly robust to islanding or targeted attacks. In addition to shedding light on self-optimization in natural systems, grass-roots optimization can also support the parallelizable and scalable engineering of man-made systems.

The ability for large systems of dynamical units to self-organize and produce robust collective behavior continues to drive a large body of research [1, 2]. Applications include cardiac dynamics [3], brain dynamics [4], cell signaling [5], and power grids [6]. Weak synchronization and desynchronization events often lead to pathological behavior, e.g., spiral wave breakup in cardiac tissue [7, 8] and black outs in power grids [9], thereby motivating *optimized* systems for strong, robust synchronization. While man-made systems such as power grids can be designed and calibrated using global structural and dynamical information [12, 13], such information is likely unavailable to naturally occurring systems. Notably, a great deal is known about how biological systems function, however comparatively little is understood about the self-optimization processes that are tasked with constructing and maintaining/repairing such systems. Prominent examples include cardiac pacemakers that initialize strongly synchronized pulses that propagate through tissue [10] and coordination of chromosomal activity through cell differentiation [11]. For synchronizing systems that rely on collective behavior, it is reasonable to assume that the related optimization mechanisms are themselves a collective, coordinated behavior. A stronger theoretical understanding of such mechanisms for collective (self) optimization will deepen our understanding of diverse types of biological (and other) systems and has the potential to revolutionize the way we engineer systems—or rather, design systems to engineer themselves. To this end, collective optimizations constitute an under-explored family of collective behavior, and there is a lack of multiscale optimization theory to provide insight into how local optimizations might coordinate to optimize globally—both in the context of synchronization and more broadly.

In this paper, we explore *grass-roots optimization* for coupled oscillator networks, whereby the parallel optimization of smaller subsystems can be coordinated to collectively optimize the global synchronization properties of the entire system. In general, *subsystems* of a network can be defined in a variety of ways: communities [14], spatially distinct regions in a geometric network [15], or other partitions of a network after embedding in a more general metric space [16]. Our

main finding is an intuitive multiscale mechanism for grass-roots optimization of synchronization that involves two steps: *local subsystem optimization*, whereby subsystems are optimized in parallel; and *global subsystem balancing*, whereby the subsystems are balanced with one another. We derive this mechanism from first principles using the Synchrony Alignment Function (SAF) framework, which provides an objective measure of a system’s synchronization properties and has been used in a number of synchronization optimization tasks [17–22]. We demonstrate the utility of grass-roots optimization across a range of networks where structural subsystems arise naturally: networks with community structure, a power grid, and noisy geometric networks that systems with spatial constraints for connections, such as calcium release sites in cardiac pacemaker cells [3] and self-coordinating chromosomes [11]. We show that the global synchronization properties of grass-roots optimized systems are nearly identical to those of globally-optimized systems, and importantly, these properties are also more robust to subsystem dismantling, e.g., due to targeted attack or intentional ‘islanding’. Grass-roots optimization provides a viable mechanism by which biological systems can robustly self-optimize and provides engineering strategies that are decentralized, parallelizable, and scalable.

We consider networks of coupled, heterogeneous phase oscillators whose dynamics are given by

$$\dot{\theta}_i = \omega_i + K \sum_{j=1}^N A_{ij} H(\theta_j - \theta_i), \quad (1)$$

where θ_i and ω_i are the phase and natural frequency of oscillator $i = 1, \dots, N$, parameter K is the global coupling strength, network structure is encoded in an adjacency matrix A , and $H(\cdot)$ is a 2π -periodic coupling function. Here, we focus on the case of unweighted, undirected networks with $A_{ij} = 1$ if oscillators i and j are connected and 0 otherwise, although these properties may be relaxed without much trouble. We also use classical Kuramoto coupling [23], given by $H(\cdot) = \sin(\cdot)$, but emphasize that one may choose other func-

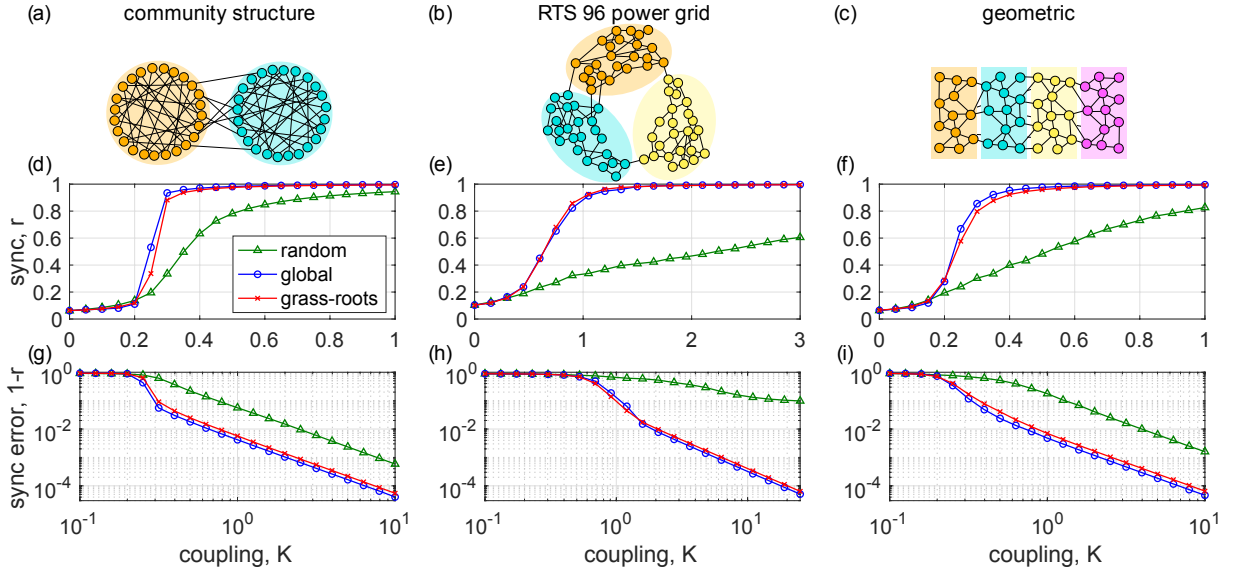


FIG. 1. *Grass-roots synchronization*. Illustrations of (a) a random network with two communities, (b) the IEEE RTS 96 power grid, and (c) a random geometric network. (d)–(f) The degree of synchronization r and (g)–(i) synchronization error $1 - r$ as a function of coupling strength K for the three respective network types with either randomly allocated frequencies (green triangles), globally-optimized frequencies (blue circles), or grass-roots optimized frequencies (red crosses).

tions H provided that $H'(0) > 0$ and $H(\Delta\theta) = 0$ for some $\Delta\theta$ near zero. Notably, phase oscillator models such as Eq. (1) have been found to be suitable models for naturally-occurring phenomena such as chromosomal coordination [11] and integrate and fire dynamics of cardiac pacemakers [24], as well as mechanical systems such as power grids [25, 26]. The degree of synchronization is measured by the magnitude $r \in [0, 1]$ of the Kuramoto order parameter $re^{i\psi} = N^{-1} \sum_{j=1}^N e^{i\theta_j}$. By linearizing around the synchronized state one obtains

$$r \approx 1 - \frac{J(\boldsymbol{\omega}, L)}{2K^2}, \text{ where } J(\boldsymbol{\omega}, L) = \frac{1}{N} \sum_{j=2}^N \frac{\langle \mathbf{v}^j, \boldsymbol{\omega} \rangle^2}{\lambda_j^2} \quad (2)$$

is the Synchrony Alignment Function (SAF) [17]. The SAF utilizes the alignment of the natural frequencies $\boldsymbol{\omega}$ with the eigenvalues $\{\lambda^j\}_{j=1}^N$ and eigenvectors $\{\mathbf{v}^j\}_{j=1}^N$ of the combinatorial Laplacian, $L = D - A$, where $D = \text{diag}(k_1, \dots, k_N)$ is a diagonal matrix that encodes the nodal degrees, $k_i = \sum_{j=1}^N A_{ij}$. Synchronization is optimized (i.e., r is maximized) by minimizing $J(\boldsymbol{\omega}, L)$, which may be done by aligning $\boldsymbol{\omega}$ with the eigenvectors of L that are associated with larger eigenvalues. Minimizing the SAF by setting $\boldsymbol{\omega} = \mathbf{v}^N$ also reveals intuitive key properties of synchrony optimized systems including degree-frequency correlations and anti-correlations between the frequencies of neighboring oscillators [17]. While such local properties are associated with synchronization, they alone do not guarantee it, nor do they offer insight toward mesoscale/multiscale properties and mechanisms enabling collective optimization.

We now present a method for grass-roots optimization of synchronization, including a multiscale mechanism in which subsystems coordinate local optimizations to optimize a sys-

tem’s global synchronization properties. We will present a detailed derivation later, and first summarize our main findings and implications. We consider networks that can be partitioned into C subsystems such that the adjacency matrix A may be rewritten in a block form $A = A_D + B$, where $A_D = \text{diag}(A^{(1)}, \dots, A^{(C)})$ is a block-diagonal matrix containing the subsystems’ separate adjacency matrices, and the off-diagonal blocks of B encode edges between subsystems. We assume that the blocks in B are sparser than the diagonal blocks in A_D . For each subsystem s , we define its associated combinatorial Laplacian matrix $L^{(s)}$ and its associated vector $\boldsymbol{\omega}^{(s)}$ of frequencies. As we will show below, *under the condition where the subsystems’ mean oscillator frequencies are equal*, then the SAF for the full system may be approximated by a linear combination of the subsystem-specific SAFs,

$$J(\boldsymbol{\omega}, L) \approx \eta_1 J(\boldsymbol{\omega}^{(1)}, L^{(1)}) + \dots + \eta_C J(\boldsymbol{\omega}^{(C)}, L^{(C)}), \quad (3)$$

where η_s is the fraction of nodes in subsystem s . This result leads to the following multiscale mechanism for grass-roots optimization: (i) *Global balancing of subsystems*: achieve a balanced set of local mean frequencies across all C subsystems, i.e., minimize $\max_{s,s'} |\langle \boldsymbol{\omega}^{(s)} \rangle - \langle \boldsymbol{\omega}^{(s')} \rangle|$; (ii) *Local optimization of subsystems*: optimize the local SAFs, i.e., minimize $J(\boldsymbol{\omega}^{(s)}, L^{(s)})$ for each s . This framework is flexible and may be used under a wide range of application-specific constraints. Notably, these two intuitive steps are a plausible mechanism that can be utilized by biological (and other natural) systems to self-optimize using local/global mechanisms, and it helps fill the theoretical gap between existing (global) optimization theory and known (local) heuristic properties that promote synchrony (e.g., degree-frequency correlations).

We now illustrate the effectiveness of grass-roots optimization across three classes of networks: (i) networks with community structure (which are generated by the stochastic block model [27], contain two communities of sizes $N^{(1:2)} = 100$, and have mean intra-degree $\langle k^{(1:2)} \rangle = 5$ and mean inter-degree $\langle k^{(12)} \rangle = 1$); (ii) the RTS 96 power grid [28]; (iii) and noisy geometric networks [29] (which consist of $N = 200$ nodes placed uniformly within a 4×1 box with 95% of links placed between the closest possible nodes pairs and the other 5% of links placed randomly, resulting in a mean degree of $\langle k \rangle = 8$). As shown in Figs. 1(a)–(c), we partition the three classes of networks into two, three, and four subsystems, respectively. (The four subsystems of the geometric networks are defined by the \pm sign combinations in the first two non-trivial eigenvectors of L .)

For each network, we assume that natural frequencies are given and cannot be modified, but may be rearranged. Thus, a global balance between subsystems [step (i)] may be obtained by shuffling frequencies between subsystems, while the subsystems may be locally optimized [step (ii)] by then shuffling frequencies within each subsystem. To optimize each network, we use an accept-reject algorithm, proposing 5×10^4 switches between randomly chosen pairs of frequencies and accepting switches that decrease the SAF. In Figs. 1(d)–(f), we plot the synchronization profile, r vs K , for systems with randomly allocated frequencies (green triangles), globally optimized frequencies (blue circles) and grass-roots optimized frequencies (red crosses) for the three classes of networks. All data points are averaged across 50 random networks and natural frequency realizations (drawn from the standard normal distribution) except for the power grid, where the same network is used throughout. Note the comparably strong synchronization properties for both the global and grass-roots optimized cases. To differentiate the two cases we plot the synchronization error $1 - r$ vs K in a log-log scale in Figs. 1(g)–(i), revealing that grass-roots optimization is very effective across a wide range of network structures.

Next we show that grass-roots optimized networks outperform globally optimized networks when subsystems are isolated from one another or otherwise dismantled by a targeted attack. For instance, modern power grids feature microgrids that are smaller subsystems that may be separated, i.e., “islanded”, from the larger grid [25]. We predict such a feature to be advantageous to synchronizing biological processes, which is a main motivator for our work. As an example, we consider the RTS 96 power grid before and after the islanding of three subsystems [as indicated in Fig. 2(c)]. In Fig. 1(a) we plot time series of three local order parameters for system designed using global (solid blue) and grass-root (dashed red) optimization. We use $K = 1$ and normally-distributed frequencies. Edges between subsystems are removed at time $t = 0$. Before islanding ($t < 0$) both cases display strong synchronization properties. After islanding ($t \geq 0$) the globally-optimized system displays significantly weaker synchronization properties and a desynchronization event (indicated by oscillations). On the other hand, the grass-roots optimized system maintains

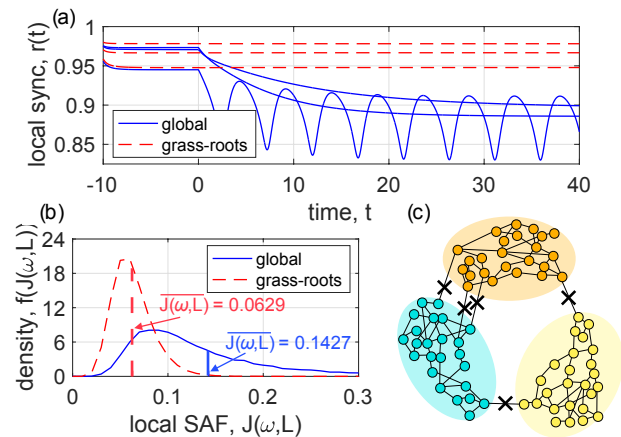


FIG. 2. *Robustness to islanding and target attacks.* (a) Example of local (subsystem) order parameters for the RTS 96 power grid before ($t < 0$) and after ($t \geq 0$) islanding for global (solid blue) and grass-roots (dashed red) optimization. (b) Density of local (subsystem) SAFs after islanding for global (solid blue) and grass-roots (dashed red) optimization. (c) Illustration of the islanded subsystems in the RTS 96 power grid.

its strong synchronization properties. This is further demonstrated in Fig. 2(b), where we plot the density of local, i.e., subsystem-specific, SAFs for globally (solid blue) and grass-roots (dashed red) optimized systems obtained from 10^4 realizations. We indicate the respective means $\overline{J(\omega, L)} = 0.1427$ and 0.0629 of the local SAFs for the globally and grass-roots optimized cases with vertical lines.

We conclude by finally presenting our local approximation of the SAF, which has allowed us to identify the multiscale mechanism (i.e., steps i-ii) underlying grass-roots optimization. For simplicity, we first consider the case of two subsystems, leaving further generalization to the Supplemental Material (SM). Writing the adjacency matrix as $A = \begin{bmatrix} A^{(1)} & B^{(12)} \\ B^{(12)T} & A^{(2)} \end{bmatrix}$, where $A^{(1)} \in \mathbb{R}^{N_1 \times N_1}$, $A^{(2)} \in \mathbb{R}^{N_2 \times N_2}$, $B^{(12)} \in \mathbb{R}^{N_1 \times N_2}$, and N_1 and N_2 are the sizes of the respective subsystems, the Laplacian is given by $L = L_0 + L_B$, where $L_0 = \begin{bmatrix} L^{(1)} & 0 \\ 0 & L^{(2)} \end{bmatrix}$, $L_B = \begin{bmatrix} D_{B^{(12)}} & -B^{(12)} \\ -B^{(12)T} & D_{B^{(12)T}} \end{bmatrix}$, and $L^{(1,2)} = D^{(1,2)} - A^{(1,2)}$ with diagonal matrices $D_{B^{(12)}}$ and $D_{B^{(12)T}}$ whose entries correspond to row sums of $B^{(12)}$ and $B^{(12)T}$, respectively. We assume $B^{(12)}$ to be sparser than $A^{(1)}$ and $A^{(2)}$ so that $\|L_B\| \ll \|L_0\|$ under a suitable matrix norm (e.g., the Frobenius norm). We then define $\Delta L = (\|L_0\|/\|L_B\|)L_B$ so that $L(\epsilon) = L_0 + \epsilon\Delta L$ recovers the original network structure for the choice $\epsilon = \|L_B\|/\|L_0\| \ll 1$.

Next, we discuss the spectral properties of L_0 . Since this matrix encodes the two subsystems in isolation, its eigenvalue spectrum is the union of the eigenvalue spectrum of $L^{(1)}$ and $L^{(2)}$. Specifically, ordering the eigenvalues of $L^{(1)}$ and $L^{(2)}$, respectively, $0 = \mu_1 < \mu_2 \leq \dots \leq \mu_{N_1}$ and $0 = \nu_1 < \nu_2 \leq \dots \leq \nu_{N_2}$ (where we assume that the subsystems are themselves connected), this implies that L_0 has two zero eigenvalues, $\lambda_1 = \lambda_2 = 0$, and the rest

are positive. Since 0 is a repeated eigenvalue of L_0 , its nullspace requires some care. Rather than choosing eigenvectors $\mathbf{v}^1 \propto [\mathbf{1}, \mathbf{0}]^T$ and $\mathbf{v}^2 \propto [\mathbf{0}, \mathbf{1}]^T$, whose entries are constant within one subsystem and zero within the other, it is advantageous to instead choose $\mathbf{v}^1 = \frac{1}{\sqrt{N}}[\mathbf{1}, \mathbf{1}]^T$ and $\mathbf{v}^2 = \frac{\sqrt{N_1 N_2}}{N}[\mathbf{1}/N_1, -\mathbf{1}/N_2]^T$ so that \mathbf{v}^1 is independent of ϵ and characterizes the nullspace of $L(\epsilon)$, and \mathbf{v}^2 is associated with an eigenvalue that converges to 0 as $\epsilon \rightarrow 0$ but is strictly positive for $\epsilon > 0$. The other $N - 2$ eigenvectors of L_0 are given by $\{\mathbf{v}^j\}_{j=3}^N = \{[\mathbf{u}^j, \mathbf{0}]^T\}_{j=2}^{N_1} \cup \{[\mathbf{0}, \mathbf{x}^j]^T\}_{j=2}^{N_2}$, where $\{\mathbf{u}^j\}_{j=1}^{N_1}$ and $\{\mathbf{x}^j\}_{j=1}^{N_2}$ are the eigenvectors of $L^{(1)}$ and $L^{(2)}$.

Considering $0 < \epsilon \ll 1$, each eigenvalue of $L(\epsilon)$ varies

continuously with ϵ [30], so we may write $\lambda_j(\epsilon) = \lambda_j + \epsilon \delta \lambda_j^{(1)} + \epsilon^2 \delta \lambda_j^{(2)} + \mathcal{O}(\epsilon^3)$. We similarly assume $\mathbf{v}^j(\epsilon) = \mathbf{v}^j + \epsilon \delta \mathbf{v}^{j(1)} + \epsilon^2 \delta \mathbf{v}^{j(2)} + \mathcal{O}(\epsilon^3)$. Since $\lambda_2(\epsilon) \ll 1$ and $\lambda_j(\epsilon) \sim 1$ for $j = 3, \dots, N$, the term associated with $j = 2$ needs to be treated separately from the others, and

$$J(\boldsymbol{\omega}, L(\epsilon)) = \frac{1}{N} \left(\frac{\langle \boldsymbol{\omega}, \mathbf{v}^2(\epsilon) \rangle}{\lambda_2(\epsilon)} \right)^2 + \frac{1}{N} \sum_{j=3}^N \left(\frac{\langle \boldsymbol{\omega}, \mathbf{v}^j(\epsilon) \rangle}{\lambda_j(\epsilon)} \right)^2. \quad (4)$$

Upon expanding the $N - 1$ terms contributing to the SAF in Eq. (4), we find that they all take a similar form except for a factor of ϵ ,

$$\begin{aligned} \left(\frac{\langle \boldsymbol{\omega}, \mathbf{v}^j(\epsilon) \rangle}{\lambda_j(\epsilon)} \right)^2 &= \epsilon^{\alpha_j} \left(\frac{\langle \boldsymbol{\omega}, \mathbf{v}^j \rangle^2}{(\lambda_j)^2} \right) + \epsilon^{1+\alpha_j} \left(\frac{2\langle \boldsymbol{\omega}, \mathbf{v}^j \rangle \langle \boldsymbol{\omega}, \delta \mathbf{v}^{j(1)} \rangle}{(\lambda_j)^2} - \frac{2\delta \lambda_j^{(1)} \langle \boldsymbol{\omega}, \mathbf{v}^j \rangle^2}{(\lambda_j)^3} \right) \\ &+ \epsilon^{2+\alpha_j} \left(\frac{\langle \boldsymbol{\omega}, \delta \mathbf{v}^{j(1)} \rangle^2 + 2\langle \boldsymbol{\omega}, \mathbf{v}^j \rangle \langle \boldsymbol{\omega}, \delta \mathbf{v}^{j(2)} \rangle}{(\lambda_j)^2} - \frac{4\delta \lambda_j^{(1)} \langle \boldsymbol{\omega}, \mathbf{v}^j \rangle \langle \boldsymbol{\omega}, \delta \mathbf{v}^{j(1)} \rangle}{(\lambda_j)^3} + \frac{(3(\delta \lambda_j^{(1)})^2 - 2\lambda_j \delta \lambda_j^{(2)}) \langle \boldsymbol{\omega}, \mathbf{v}^j \rangle^2}{(\lambda_j)^4} \right) + \mathcal{O}(\epsilon^{3+\alpha_j}), \end{aligned} \quad (5)$$

where α_j is a term that equals -2 when $j = 2$ and 0 when $j \geq 3$. Due to the different scaling with ϵ , the terms associated with $j = 2$ are much larger than those for $j \geq 3$. Inserting Eq. (5) into Eq. (4) yields

$$\begin{aligned} J(\boldsymbol{\omega}, L(\epsilon)) &= N^{-1} \epsilon^{-2} \left(\frac{\langle \boldsymbol{\omega}, \mathbf{v}^2 \rangle^2}{(\delta \lambda_2^{(1)})^2} \right) + N^{-1} \epsilon^{-1} \left(\frac{2\langle \boldsymbol{\omega}, \mathbf{v}^2 \rangle \langle \boldsymbol{\omega}, \delta \mathbf{v}^{2(1)} \rangle}{(\delta \lambda_2^{(1)})^2} - \frac{2\delta \lambda_2^{(2)} \langle \boldsymbol{\omega}, \mathbf{v}^2 \rangle^2}{(\delta \lambda_2^{(1)})^3} \right) \\ &+ N^{-1} \left(\frac{\langle \boldsymbol{\omega}, \delta \mathbf{v}^{2(1)} \rangle^2 + 2\langle \boldsymbol{\omega}, \mathbf{v}^2 \rangle \langle \boldsymbol{\omega}, \delta \mathbf{v}^{2(2)} \rangle}{(\delta \lambda_2^{(1)})^2} - \frac{4\delta \lambda_2^{(2)} \langle \boldsymbol{\omega}, \mathbf{v}^2 \rangle \langle \boldsymbol{\omega}, \delta \mathbf{v}^{2(1)} \rangle}{(\delta \lambda_2^{(1)})^3} + \frac{(3(\delta \lambda_2^{(2)})^2 - 2\delta \lambda_2^{(1)} \delta \lambda_2^{(3)}) \langle \boldsymbol{\omega}, \mathbf{v}^2 \rangle^2}{(\delta \lambda_2^{(1)})^4} \right) \\ &+ \eta_1 J(\boldsymbol{\omega}^{(1)}, L_1) + \eta_2 J(\boldsymbol{\omega}^{(2)}, L_2) + \epsilon \left[N^{-1} \sum_{j=3}^N \left(\frac{2\langle \boldsymbol{\omega}, \mathbf{v}^j \rangle \langle \boldsymbol{\omega}, \delta \mathbf{v}^{j(1)} \rangle}{(\lambda_j)^2} - \frac{2\delta \lambda_j^{(1)} \langle \boldsymbol{\omega}, \mathbf{v}^j \rangle^2}{(\lambda_j)^3} \right) \right] + \mathcal{O}(N^{-1} \epsilon, \epsilon^2), \end{aligned} \quad (6)$$

where we have used that $\frac{1}{N} \sum_{j=3}^N \frac{\langle \boldsymbol{\omega}, \mathbf{v}^j \rangle^2}{\lambda_j^2} = \eta_1 J(\boldsymbol{\omega}^{(1)}, L^{(1)}) + \eta_2 J(\boldsymbol{\omega}^{(2)}, L^{(2)})$. While Eq. (6) may appear daunting, the key insight is the presence of an inner product $\langle \boldsymbol{\omega}, \mathbf{v}^2 \rangle$ in several leading-order terms. Recalling the structure of \mathbf{v}^2 , and writing $\boldsymbol{\omega} = [\boldsymbol{\omega}^{(1)}, \boldsymbol{\omega}^{(2)}]^T$, where $\boldsymbol{\omega}^{(1)}$ and $\boldsymbol{\omega}^{(2)}$ are the frequency vectors corresponding to the two subsystems, we have that $\langle \boldsymbol{\omega}, \mathbf{v}^2 \rangle = \sqrt{\eta_1 \eta_2} (\langle \boldsymbol{\omega}^{(1)} \rangle - \langle \boldsymbol{\omega}^{(2)} \rangle)$. Thus, if the subsystems' mean frequencies can be engineered to match, $\langle \boldsymbol{\omega}^{(1)} \rangle = \langle \boldsymbol{\omega}^{(2)} \rangle$, then many terms vanish to yield

$$\begin{aligned} J(\boldsymbol{\omega}, L(\epsilon)) &= \eta_1 J(\boldsymbol{\omega}^{(1)}, L_1) + \eta_2 J(\boldsymbol{\omega}^{(2)}, L_2) \\ &+ \epsilon \left[N^{-1} \sum_{j=3}^N \left(\frac{2\langle \boldsymbol{\omega}, \mathbf{v}^j \rangle \langle \boldsymbol{\omega}, \delta \mathbf{v}^{j(1)} \rangle}{(\lambda_j)^2} - \frac{2\delta \lambda_j^{(1)} \langle \boldsymbol{\omega}, \mathbf{v}^j \rangle^2}{(\lambda_j)^3} \right) \right] \\ &+ N^{-1} \left(\frac{\langle \boldsymbol{\omega}, \delta \mathbf{v}^{2(1)} \rangle^2}{(\delta \lambda_2^{(1)})^2} \right) + \mathcal{O}(N^{-1} \epsilon, \epsilon^2), \end{aligned} \quad (7)$$

which recovers Eq. (3) to leading order for the case of $C = 2$ subsystems. See the SM for further generalization insights.

While recent progress has been made in optimizing collective behavior in complex systems, the resulting techniques and methodologies rely largely on global network information. These approaches express certain local properties such as correlations between nodal degrees and natural frequencies [17, 18], however such properties alone do not optimize systems. This leaves open the critical question of how naturally-occurring systems tune their own structure and dynamics to self-optimize, and it is reasonable to consider that the optimization itself is a collective behavior.

Grass-roots optimization is a multiscale mechanism for coordinating and optimizing the local synchronization properties of a network's subsystems and is a plausible mechanism for collective (self) optimization within naturally-occurring systems that have access to only local information, such as car-

diac pacemakers [3] and genetic oscillators [11]. It can also support the design of decentralized, parallelizable and scalable algorithms to engineer man-made systems that are robust to network dismantling. Notably, these very same features may have provided an evolutionary advantage for biological systems that crucially depend on synchronization.

PRC was supported by the Interdisciplinary Science Program and Summer Research Program at Trinity College. PSS was supported by NSF grant MCB-2126177. DT was supported by NSF grant DMS-2052720 and Simons Foundation award #578333.

* persebastian.skardal@trincoll.edu

- [1] A. Pikovsky, M. Rosenblum, and J. Kurths, *Synchronization: a universal concept in nonlinear sciences* (Cambridge University Press, 2003).
- [2] S. H. Strogatz, *Sync: The emerging science of spontaneous order* (Penguin UK, 2004).
- [3] R. Bychkov, M. Juhaszova, K. Tsutsui, C. Coletta, M. D. Stern, V. A. Maltsev, and E. G. Lakatta, Synchronized Cardiac Impulses Emerge From Heterogeneous Local Calcium Signals Within and Among Cells of Pacemaker Tissue, *JACC Clin. Electrophysiol.* **6**, 907 (2020).
- [4] N. Kopell, G. B. Ermentrout, M. A. Whittington, and R. D. Traub, Gamma rhythms and beta rhythms have different synchronization properties, *Proc. Natl. Acad. Sci. U.S.A.* **97**, 1867 (2000).
- [5] A. Prindle, P. Samayoa, I. Razinkov, T. Danino, L. S. Tsimring, and J. Hasty, A sensing array of radically couples genetic ‘biopixels’, *Nature* **481**, 39 (2012).
- [6] M. Rohden, A. Sorge, M. Timme, and D. Witthaut, Self-organized synchronization in decentralized power grids, *Phys. Rev. Lett.* **109**, 064101 (2012).
- [7] F. H. Fenton, E. M. Cherry, H. M. Hastings, and S. J. Evans, Multiple mechanisms of spiral wave breakup in a model of cardiac electrical activity, *Chaos* **12**, 852 (2002).
- [8] A. V. Panfilov, R. H. Keldermann, and M. P. Nash, Drift and breakup of spiral waves in reaction–diffusion–mechanics systems, *Proc. Natl. Acad. Sci. U.S.A.* **104**, 7922 (2007)
- [9] F. Dörfler, M. Chertkov, and F. Bullo, Synchronization in complex oscillator networks and smart grids, *Proc. Natl. Acad. Sci. U.S.A.* **110**, 1005 (2013).
- [10] M. E. Mangoni and J. Nargeot, Genesis and regulation of the heart automaticity, *Physiol. Rev.* **88**, 919 (2008).
- [11] I. Rajapakse, M. D. Perlman, D. Scalzo, C. Kooperberg, M. Groudine, and S. T. Kosak, The emergence of lineage-specific chromosomal topologies from coordinate gene regulation, *Proc. Natl. Acad. Sci. U.S.A.* **106**, 6679 (2009).
- [12] L. M. Pecora and T. L. Carroll, Master stability function for synchronized coupled systems, *Phys. Rev. Lett.* **80**, 2109 (1998).
- [13] T. Nishikawa and A. Motter, Synchronization is optimal in non-diagonalizable networks, *Phys. Rev. E* **73**, 065106(R) (2006).
- [14] M. Girvan and M. E. J. Newman, Community structure in social and biological networks, *Proc. Natl. Acad. Sci. U.S.A.* **99**, 7821 (2002).
- [15] M. Barthélemy, *Spatial Networks*, *Phys. Rep.* **499**, 1 (2011).
- [16] R. R. Coifman, S. Lafon, A. B. Lee, M. Maggioni, B. Nadler, F. Warner, and S. W. Zucker, Geometric diffusions as a tool for harmonic analysis and structure definition of data: Diffusion maps, *Proc. Natl. Acad. Sci. U.S.A.* **102**, 7426 (2005).
- [17] P. S. Skardal, D. Taylor, and J. Sun, Optimal synchronization of complex networks, *Phys. Rev. Lett.* **113**, 144101 (2014).
- [18] P. S. Skardal, D. Taylor, and J. Sun, Optimal synchronization of directed complex networks, *Chaos* **26**, 094807 (2016).
- [19] D. Taylor, P. S. Skardal, and J. Sun, Synchronization of heterogeneous oscillators under network modifications: Perturbation and optimization of the synchrony alignment function, *SIAM J. Appl. Math.* **76**, 1984 (2016).
- [20] L. Arola-Fernández, P. S. Skardal, and A. Arenas, Geometric unfolding of synchronization dynamics on networks, *Chaos* **31**, 061105 (2021).
- [21] P. S. Skardal, R. Sevilla-Escoboza, V. Vera-Ávila, and J. M. Buldú, Optimal phase synchronization in networks of phase-coherent chaotic oscillators, *Chaos* **27**, 013111 (2017).
- [22] P. S. Skardal, D. Taylor, and J. Sun, Synchronization of network-coupled oscillators with uncertain dynamics, *SIAM J. Appl. Math.* **79**, 2409 (2019).
- [23] Y. Kuramoto, *Chemical oscillations, waves, and turbulence* (Springer, 2012).
- [24] A. Politi and M. Rosenblum, Equivalence of phase-oscillator and integrate-and-fire models, *Phys. Rev. E* **91**, 042916 (2015).
- [25] J. W. Simpson-Porco, F. Dörfler, and F. Bullo, Synchronization and power sharing for droop-controlled inverters in islanded microgrids, *Automatica* **49**, 2603 (2013).
- [26] P. S. Skardal and A. Arenas, Control of coupled oscillator networks with application to microgrid technologies, *Sci. Adv.* **1**, e1500339 (2015).
- [27] P. W. Holland, K. B. Laskey, and S. Leinhardt, Stochastic block-models: First steps, *Soc. Networks* **5**, 109 (1983).
- [28] C. Grigg et al., The IEEE Reliability Test System—1996. A report prepared by the Reliability Test System Task Force of the Application of Probability Methods Subcommittee, *IEEE Trans. Power Syst.* **14**, 1010 (1999).
- [29] D. Taylor, F. Klimm, H. A. Harrington, M. Kramar, K. Mischaikow, M. A. Porter, and P.J. Mucha, Topological data analysis of contagion maps for examining spreading processes on networks, *Nat. Commun.* **6**, 7723 (2015).
- [30] T. Kato, *Perturbation theory for linear operators, vol. 132* (Springer Science & Business Media, 2013).

Supplemental Material: Grass-roots optimization of coupled oscillator networks

In this Supplemental Material we generalize the local approximation of the SAF for more than two subsystems. First we present the full derivation of the approximation for the case of three subsystems, and then we discuss the generalization to an arbitrary number of subsystems.

LOCAL APPROXIMATION OF THE SAF FOR NETWORKS WITH THREE SUBSYSTEMS

To provide insight into systems with more than two subsystems, we present here the case of three subsystems and derive a local approximation to the SAF analogous to the one which we presented in the main text. In this case the network adjacency matrix can be written in block form as

$$A = \begin{bmatrix} A^{(1)} & B^{(12)} & B^{(13)} \\ B^{(12)T} & A^{(2)} & B^{(23)} \\ B^{(13)T} & B^{(23)T} & A^{(3)} \end{bmatrix}, \quad (1)$$

where $A^{(1)}$, $A^{(2)}$, and $A^{(3)}$ are the adjacency matrices for the three subsystems and $B^{(12)}$, $B^{(13)}$, and $B^{(23)}$ captures the connections between the respective subsystems. We denote the sizes of the three subsystems by N_1 , N_2 , and N_3 so that $A^{(1)} \in \mathbb{R}^{N_1 \times N_1}$, $A^{(2)} \in \mathbb{R}^{N_2 \times N_2}$, $A^{(3)} \in \mathbb{R}^{N_3 \times N_3}$, $B^{(12)} \in \mathbb{R}^{N_1 \times N_2}$, $B^{(13)} \in \mathbb{R}^{N_1 \times N_3}$, and $B^{(23)} \in \mathbb{R}^{N_2 \times N_3}$. We are interested then in the perturbed combinatorial Laplacian, given by

$$L(\epsilon) = L_0 + \epsilon \Delta L, \quad (2)$$

where

$$L_0 = \begin{bmatrix} L^{(1)} & 0 & 0 \\ 0 & L^{(2)} & 0 \\ 0 & 0 & L^{(3)} \end{bmatrix}, \quad (3)$$

$\Delta L = (\|L_0\|/\|L_B\|)L_B$, and

$$L_B = \begin{bmatrix} D_{B^{(12)}+B^{(13)}} & -B^{(12)} & -B^{(13)} \\ -B^{(12)T} & D_{B^{(12)T}+B^{(23)}} & -B^{(23)} \\ -B^{(13)T} & -B^{(23)T} & D_{B^{(13)T}+B^{(23)T}} \end{bmatrix}. \quad (4)$$

Once again, the choice $\epsilon = \|L_B\|/\|L_0\| \ll 1$ recovers the original Laplacian matrix.

As in the two-subsystem case, it is useful to first discuss the spectral properties of L_0 . Since it is a block-diagonal matrix, its eigenvalues are given by the union of the eigenvalues of the respective blocks,

$$\{\lambda_j\}_{j=1}^N = \{\mu_j\}_{j=1}^{N_1} \cup \{\nu_j\}_{j=1}^{N_2} \cup \{\eta_j\}_{j=1}^{N_3}, \quad (5)$$

where $\{\mu_j\}_{j=1}^{N_1}$ denotes the eigenvalues of $L^{(1)}$, $\{\nu_j\}_{j=1}^{N_2}$ denotes the eigenvalues of $L^{(2)}$, and $\{\eta_j\}_{j=1}^{N_3}$ denotes the eigenvalues of $L^{(3)}$. The associated eigenvectors are given by

$$\{\mathbf{v}^j\}_{j=1}^N = \left\{ \begin{bmatrix} \mathbf{u}^j \\ \mathbf{0} \\ \mathbf{0} \end{bmatrix} \right\}_{j=1}^{N_1} \cup \left\{ \begin{bmatrix} \mathbf{0} \\ \mathbf{x}^j \\ \mathbf{0} \end{bmatrix} \right\}_{j=1}^{N_2} \cup \left\{ \begin{bmatrix} \mathbf{0} \\ \mathbf{0} \\ \mathbf{y}^j \end{bmatrix} \right\}_{j=1}^{N_3}. \quad (6)$$

where $\{\mathbf{u}^j\}_{j=1}^{N_1}$, $\{\mathbf{x}^j\}_{j=1}^{N_2}$, and $\{\mathbf{y}^j\}_{j=1}^{N_3}$ are the associated eigenvectors for $L^{(1)}$, $L^{(2)}$, and $L^{(3)}$, respectively. The most critical observation to make is that each diagonal block of L_0 has a trivial eigenvalue, namely, $\mu_1, \nu_1, \eta_1 = 0$, so the nullspace of L_0 is three-dimensional since it has a triple eigenvalue degeneracy at $\lambda_{1,2,3} = 0$. It is then convenient to rewrite the basis vectors for this trivial eigenspace using the following eigenvectors:

$$\mathbf{v}^1 = \frac{1}{\sqrt{N}} \begin{bmatrix} \mathbf{1} \\ \mathbf{1} \\ \mathbf{1} \end{bmatrix}, \quad \mathbf{v}^2 = \frac{\sqrt{N_1 N_2}}{N_1 + N_2} \begin{bmatrix} \mathbf{1}/N_1 \\ -\mathbf{1}/N_2 \\ \mathbf{0} \end{bmatrix}, \quad \mathbf{v}^3 = \frac{\sqrt{N_2 N_3}}{N_2 + N_3} \begin{bmatrix} \mathbf{0} \\ \mathbf{1}/N_2 \\ -\mathbf{1}/N_3 \end{bmatrix}, \quad (7)$$

where, similar to the two subsystem case, \mathbf{v}^1 is the constant-valued eigenvector that is associated with the synchronization manifold and whose eigenvalue $\lambda_1 = 0$ remains constant as ϵ increases (i.e., $v^1(\epsilon) = v^1$ regardless of ϵ). On the other hand, \mathbf{v}^2 and \mathbf{v}^3 will play important roles in the perturbation analysis since $\lambda_2(\epsilon)$ and $\lambda_3(\epsilon)$ must take positive values for any $\epsilon > 0$.

We note that the vector $\sqrt{N_1 N_3}/(N_1 + N_3) \begin{bmatrix} \mathbf{1}/N_1 \\ \mathbf{0} \\ -\mathbf{1}^T/N_3 \end{bmatrix}$ may also be used in place of either \mathbf{v}^2 or \mathbf{v}^3 , but as it is just a linear combination of the two vectors already chosen, it yields the same results given below.

Given the initial spectral properties of L_0 , we consider the following perturbative expansions. Specifically, for the eigenvalues of $L(\epsilon)$ we have

$$\lambda_j(\epsilon) = \epsilon \delta \lambda_j^{(1)} + \epsilon^2 \delta \lambda_j^{(2)} + \mathcal{O}(\epsilon^3), \quad (8)$$

for $j = 2, 3$ and

$$\lambda_j(\epsilon) = \lambda_j + \epsilon \delta \lambda_j^{(1)} + \epsilon^2 \delta \lambda_j^{(2)} + \mathcal{O}(\epsilon^3), \quad (9)$$

for $j = 4, \dots, N$. We again assume that the eigenvectors of $L(\epsilon)$ are continuously differentiable to approximate

$$\mathbf{v}^j(\epsilon) = \mathbf{v}^j + \epsilon \delta \mathbf{v}^{j(1)} + \epsilon^2 \delta \mathbf{v}^{j(2)} + \mathcal{O}(\epsilon^3). \quad (10)$$

for $j = 2, \dots, N$.

Our primary interest is the SAF of the perturbed network, and as we did in the two subsystem case with the term associated with $j = 2$, here we will treat the terms associated with $j = 2$ and 3 separately:

$$J(\boldsymbol{\omega}, L(\epsilon)) = \frac{1}{N} \left(\frac{\langle \boldsymbol{\omega}, \mathbf{v}^2(\epsilon) \rangle}{\lambda_2(\epsilon)} \right)^2 + \frac{1}{N} \left(\frac{\langle \boldsymbol{\omega}, \mathbf{v}^3(\epsilon) \rangle}{\lambda_3(\epsilon)} \right)^2 + \frac{1}{N} \sum_{j=4}^N \left(\frac{\langle \boldsymbol{\omega}, \mathbf{v}^j(\epsilon) \rangle}{\lambda_j(\epsilon)} \right)^2. \quad (11)$$

We now consider the contribution of these different terms. Beginning with the terms associated with $j = 2$ and 3, insert Eqs. (8) and (10) into the relevant terms in Eq. (11), expand, and collect similar terms to obtain

$$\begin{aligned} \frac{1}{N} \left(\frac{\langle \boldsymbol{\omega}, \mathbf{v}^j(\epsilon) \rangle}{\lambda_j(\epsilon)} \right)^2 &= N^{-1} \epsilon^{-2} \left(\frac{\langle \boldsymbol{\omega}, \mathbf{v}^j \rangle^2}{(\delta \lambda_j^{(1)})^2} \right) + N^{-1} \epsilon^{-1} \left(\frac{2 \langle \boldsymbol{\omega}, \mathbf{v}^j \rangle \langle \boldsymbol{\omega}, \delta \mathbf{v}^{j(1)} \rangle}{(\delta \lambda_j^{(1)})^2} - \frac{2 \delta \lambda_j^{(2)} \langle \boldsymbol{\omega}, \mathbf{v}^j \rangle^2}{(\delta \lambda_j^{(1)})^3} \right) \\ &+ N^{-1} \left(\frac{\langle \boldsymbol{\omega}, \delta \mathbf{v}^{j(1)} \rangle^2 + 2 \langle \boldsymbol{\omega}, \mathbf{v}^j \rangle \langle \boldsymbol{\omega}, \delta \mathbf{v}^{j(2)} \rangle}{(\delta \lambda_j^{(1)})^2} - \frac{4 \delta \lambda_j^{(2)} \langle \boldsymbol{\omega}, \mathbf{v}^j \rangle \langle \boldsymbol{\omega}, \delta \mathbf{v}^{j(1)} \rangle}{(\delta \lambda_j^{(1)})^3} \right. \\ &\left. + \frac{(3(\delta \lambda_j^{(2)})^2 - 2 \delta \lambda_j^{(1)} \delta \lambda_j^{(3)}) \langle \boldsymbol{\omega}, \mathbf{v}^j \rangle^2}{(\delta \lambda_j^{(1)})^4} \right) + \mathcal{O}(N^{-1} \epsilon). \end{aligned} \quad (12)$$

On the other hand, for $j = 4, \dots, N$, we insert Eqs. (9) and (10) into the relevant terms in Eq. (11), expand, and collect similar terms to obtain

$$\begin{aligned} \frac{1}{N} \left(\frac{\langle \boldsymbol{\omega}, \mathbf{v}^j(\epsilon) \rangle}{\lambda_j(\epsilon)} \right)^2 &= N^{-1} \left(\frac{\langle \boldsymbol{\omega}, \mathbf{v}^j \rangle^2}{(\lambda_j)^2} \right) + N^{-1} \epsilon \left(\frac{2 \langle \boldsymbol{\omega}, \mathbf{v}^j \rangle \langle \boldsymbol{\omega}, \delta \mathbf{v}^{j(1)} \rangle}{(\lambda_j)^2} - \frac{2 \delta \lambda_j^{(1)} \langle \boldsymbol{\omega}, \mathbf{v}^j \rangle^2}{(\lambda_j)^3} \right) \\ &+ N^{-1} \epsilon^2 \left(\frac{\langle \boldsymbol{\omega}, \delta \mathbf{v}^{j(1)} \rangle^2 + 2 \langle \boldsymbol{\omega}, \mathbf{v}^j \rangle \langle \boldsymbol{\omega}, \delta \mathbf{v}^{j(2)} \rangle}{(\lambda_j)^2} - \frac{4 \delta \lambda_j^{(1)} \langle \boldsymbol{\omega}, \mathbf{v}^j \rangle \langle \boldsymbol{\omega}, \delta \mathbf{v}^{j(1)} \rangle}{(\lambda_j)^3} \right. \\ &\left. + \frac{(3(\delta \lambda_j^{(1)})^2 - 2 \lambda_j \delta \lambda_j^{(2)}) \langle \boldsymbol{\omega}, \mathbf{v}^j \rangle^2}{(\lambda_j)^4} \right) + \mathcal{O}(N^{-1} \epsilon^3). \end{aligned} \quad (13)$$

Inserting Eqs. (12) and (13) into Eq. (11), we then obtain

$$\begin{aligned}
J(\boldsymbol{\omega}, L(\epsilon)) &= N^{-1}\epsilon^{-2} \left(\frac{\langle \boldsymbol{\omega}, \mathbf{v}^2 \rangle^2}{(\delta\lambda_2^{(1)})^2} + \frac{\langle \boldsymbol{\omega}, \mathbf{v}^3 \rangle^2}{(\delta\lambda_3^{(1)})^2} \right) \\
&+ N^{-1}\epsilon^{-1} \left(\frac{2\langle \boldsymbol{\omega}, \mathbf{v}^2 \rangle \langle \boldsymbol{\omega}, \delta\mathbf{v}^{2(1)} \rangle}{(\delta\lambda_2^{(1)})^2} - \frac{2\delta\lambda_2^{(2)} \langle \boldsymbol{\omega}, \mathbf{v}^2 \rangle^2}{(\delta\lambda_2^{(1)})^3} + \frac{2\langle \boldsymbol{\omega}, \mathbf{v}^3 \rangle \langle \boldsymbol{\omega}, \delta\mathbf{v}^{3(1)} \rangle}{(\delta\lambda_3^{(1)})^2} - \frac{2\delta\lambda_3^{(2)} \langle \boldsymbol{\omega}, \mathbf{v}^3 \rangle^2}{(\delta\lambda_3^{(1)})^3} \right) \\
&+ N^{-1} \left(\frac{\langle \boldsymbol{\omega}, \delta\mathbf{v}^{2(1)} \rangle^2 + 2\langle \boldsymbol{\omega}, \mathbf{v}^2 \rangle \langle \boldsymbol{\omega}, \delta\mathbf{v}^{2(2)} \rangle}{(\delta\lambda_2^{(1)})^2} - \frac{4\delta\lambda_2^{(2)} \langle \boldsymbol{\omega}, \mathbf{v}^2 \rangle \langle \boldsymbol{\omega}, \delta\mathbf{v}^{2(1)} \rangle}{(\delta\lambda_2^{(1)})^3} + \frac{(3(\delta\lambda_2^{(2)})^2 - 2\delta\lambda_2^{(1)}\delta\lambda_2^{(3)}) \langle \boldsymbol{\omega}, \mathbf{v}^2 \rangle^2}{(\delta\lambda_2^{(1)})^4} \right. \\
&\quad \left. + \frac{\langle \boldsymbol{\omega}, \delta\mathbf{v}^{3(1)} \rangle^2 + 2\langle \boldsymbol{\omega}, \mathbf{v}^3 \rangle \langle \boldsymbol{\omega}, \delta\mathbf{v}^{3(2)} \rangle}{(\delta\lambda_3^{(1)})^2} - \frac{4\delta\lambda_3^{(2)} \langle \boldsymbol{\omega}, \mathbf{v}^3 \rangle \langle \boldsymbol{\omega}, \delta\mathbf{v}^{3(1)} \rangle}{(\delta\lambda_3^{(1)})^3} + \frac{(3(\delta\lambda_3^{(2)})^2 - 2\delta\lambda_3^{(1)}\delta\lambda_3^{(3)}) \langle \boldsymbol{\omega}, \mathbf{v}^3 \rangle^2}{(\delta\lambda_3^{(1)})^4} \right) \\
&+ \eta_1 J(\boldsymbol{\omega}^1, L_1) + \eta_2 J(\boldsymbol{\omega}^2, L_2) + \eta_3 J(\boldsymbol{\omega}^3, L_3) + \epsilon \left[N^{-1} \sum_{j=4}^N \left(\frac{2\langle \boldsymbol{\omega}, \mathbf{v}^j \rangle \langle \boldsymbol{\omega}, \delta\mathbf{v}^{j(1)} \rangle}{(\lambda_j)^2} - \frac{2\delta\lambda_j^{(1)} \langle \boldsymbol{\omega}, \mathbf{v}^j \rangle^2}{(\lambda_j)^3} \right) \right] + \mathcal{O}(N^{-1}\epsilon, \epsilon^2),
\end{aligned} \tag{14}$$

where we have used that, for the three subsystem case, we have

$$\frac{1}{N} \sum_{j=4}^N \frac{\langle \boldsymbol{\omega}, \mathbf{v}^j \rangle^2}{\lambda_j^2} = \eta_1 J(\boldsymbol{\omega}^1, L_1) + \eta_2 J(\boldsymbol{\omega}^2, L_2) + \eta_3 J(\boldsymbol{\omega}^3, L_3). \tag{15}$$

Lastly, to complete the analysis we consider not only the contributions of $\langle \boldsymbol{\omega}, \mathbf{v}^2 \rangle$, but also $\langle \boldsymbol{\omega}, \mathbf{v}^3 \rangle$. In particular, we note that

$$\langle \boldsymbol{\omega}, \mathbf{v}^2 \rangle = \frac{\sqrt{\eta_1\eta_2}}{\eta_{12}} (\langle \omega^1 \rangle - \langle \omega^2 \rangle), \tag{16}$$

and

$$\langle \boldsymbol{\omega}, \mathbf{v}^3 \rangle = \frac{\sqrt{\eta_2\eta_3}}{\eta_{23}} (\langle \omega^2 \rangle - \langle \omega^3 \rangle), \tag{17}$$

where $\eta_{ij} = (N_i + N_j)/N$. Thus, if we may engineer the network such that $\langle \omega^1 \rangle = \langle \omega^2 \rangle = \langle \omega^3 \rangle$, then all terms in Eq. (14) with $\langle \boldsymbol{\omega}, \mathbf{v}^2 \rangle$ or $\langle \boldsymbol{\omega}, \mathbf{v}^3 \rangle$ vanish, yielding

$$\begin{aligned}
J(\boldsymbol{\omega}, L(\epsilon)) &= \eta_1 J(\boldsymbol{\omega}^1, L_1) + \eta_2 J(\boldsymbol{\omega}^2, L_2) + \eta_3 J(\boldsymbol{\omega}^3, L_3) + N^{-1} \left(\frac{\langle \boldsymbol{\omega}, \delta\mathbf{v}^{2(1)} \rangle^2}{(\delta\lambda_2^{(1)})^2} + \frac{\langle \boldsymbol{\omega}, \delta\mathbf{v}^{3(1)} \rangle^2}{(\delta\lambda_3^{(1)})^2} \right) \\
&+ \epsilon \left[N^{-1} \sum_{j=4}^N \left(\frac{2\langle \boldsymbol{\omega}, \mathbf{v}^j \rangle \langle \boldsymbol{\omega}, \delta\mathbf{v}^{j(1)} \rangle}{(\lambda_j)^2} - \frac{2\delta\lambda_j^{(1)} \langle \boldsymbol{\omega}, \mathbf{v}^j \rangle^2}{(\lambda_j)^3} \right) \right] + \mathcal{O}(N^{-1}\epsilon, \epsilon^2),
\end{aligned} \tag{18}$$

where the leading-order behavior of the perturbed SAF is simply given by a weighted average of the subsystem-specific SAFs and the weights come from their relative sizes, which is our desired result and the analogous version of Eq. (7) in the main text.

LOCAL APPROXIMATION OF THE SAF FOR NETWORKS WITH AN ARBITRARY NUMBER OF SUBSYSTEMS

Before concluding, we emphasize that the three subsystem case above informs the generalization of the local approximation to an arbitrary number of subsystems. In particular, for C subsystems, the unperturbed Laplacian L_0 will contain C diagonal blocks, each with a trivial eigenvalue. Thus, a basis for the trivial eigenspace must be chosen so that, in addition to $\mathbf{v}^1 \propto \mathbf{1}$, there

are $C - 1$ eigenvectors whose eigenvalues will become positive for positive ϵ . This can be done by choosing, for instance,

$$\mathbf{v}^2 = \begin{bmatrix} 1/N_1 \\ -1/N_2 \\ \mathbf{0} \\ \vdots \\ \mathbf{0} \end{bmatrix}, \quad \mathbf{v}^3 = \begin{bmatrix} \mathbf{0} \\ 1/N_2 \\ -1/N_3 \\ \vdots \\ \mathbf{0} \end{bmatrix}, \quad \dots, \quad \mathbf{v}^j = \begin{bmatrix} \vdots \\ 1/N_{j-1} \\ -1/N_j \\ \vdots \\ \mathbf{0} \end{bmatrix}, \quad \dots, \quad \mathbf{v}^C = \begin{bmatrix} \mathbf{0} \\ \vdots \\ \mathbf{0} \\ 1/N_{C-1} \\ -1/N_C \end{bmatrix}. \quad (19)$$

Then, after expansion, setting $\langle \omega^1 \rangle = \dots = \langle \omega^C \rangle$ causes the two lowest order contributions to $J(\boldsymbol{\omega}, L(\epsilon))$ originating from the terms associated with $j = 2, \dots, C$ to vanish, yielding, to leading order,

$$J(\boldsymbol{\omega}, L(\epsilon)) \approx \eta_1 J(\boldsymbol{\omega}^1, L^{(1)}) + \dots + \eta_C J(\boldsymbol{\omega}^C, L^{(C)}). \quad (20)$$